Journal of Colloid and Interface Science 446 (2015) 122–132

Contents lists available at ScienceDirect

Journal of Colloid and Interface Science

www.elsevier.com/locate/jcis

Regular Article

Application of green seaweed biomass for Mo^{VI} sorption from contaminated waters. Kinetic, thermodynamic and continuous sorption studies

Fernando A. Bertoni, Anabela C. Medeot, Juan C. González, Luis F. Sala, Sebastián E. Bellú *

Área Química General, Departamento de Químico-Física, Facultad de Ciencias Bioquímicas y Farmacéuticas, Universidad Nacional de Rosario, Suipacha 531, S2002LRK Rosario, Santa Fe, Argentina
Instituto de Química de Rosario-CONICET, Suipacha 570, S2002LRK Rosario, Santa Fe, Argentina

GRAPHICAL ABSTRACT

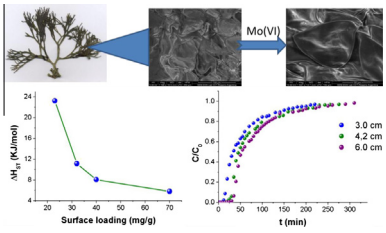

ARTICLE INFO

Article history:
Received 28 November 2014
Accepted 14 January 2015
Available online 24 January 2015

Keywords:
Molybdenum
Sorption
Green seaweed
Contamination

ABSTRACT

Spongomorpha pacifica biomass was evaluated as a new sorbent for Mo^{VI} removal from aqueous solution. The maximum sorption capacity was found to be $1.28 \times 10^6 \pm 1 \times 10^4$ mg kg^{-1} at 20 °C and pH 2.0. Sorption kinetics and equilibrium studies followed pseudo-first order and Langmuir adsorption isotherm models, respectively. FTIR analysis revealed that carboxyl and hydroxyl groups were mainly responsible for the sorption of Mo^{VI}. SEM images show that morphological changes occur at the biomass surface after Mo^{VI} sorption. Activation parameters and mean free energies obtained with Dubinin–Radushkevich isotherm model demonstrate that the mechanism of sorption process was chemical sorption. Thermodynamic parameters demonstrate that the sorption process was spontaneous, endothermic and the driven force was entropic. The isosteric heat of sorption decreases with surface loading, indicating that *S. pacifica* has an energetically non-homogeneous surface. Experimental breakthrough curves were simulated by Thomas and modified dose–response models. The bed depth service time (BDST) model was employed to scale-up the continuous sorption experiments. The critical bed depth, Z_0 was determined to be 1.7 cm. *S. pacifica* biomass showed to be a good sorbent for Mo^{VI} and it can be used in continuous treatment of effluent polluted with molybdate ions.

1. Introduction

Molybdenum is an essential trace element for both plants and animals, including humans. In animals, Mo is present as a cofactor for redox enzymes such as xanthine oxidase, and it is essential for a fine performing of these enzymes [1]. In plants, this element is necessary for the fixation of atmospheric nitrogen by bacteria at the

* Corresponding author at: Universidad Nacional de Rosario, Área Química General, Departamento de Químico-Física, Facultad de Ciencias Bioquímicas y Farmacéuticas, Suipacha 531, S2002LRK Rosario, Santa Fe, Argentina. Fax: +54 341 4350214.
E-mail addresses: bellu@iquir-conicet.gov.ar, sbellu@fbioyf.unr.edu.ar (S.E. Bellú).

http://dx.doi.org/10.1016/j.jcis.2015.01.033
0021-9797/

start of protein synthesis. Nevertheless, it is harmful at high levels. It appears to be toxic when its concentration in plants is higher than 5 μg g^{-1}, whereas potential toxicity for ruminants equals to 10 μg g^{-1} [2,3]. Owing to its high melting point, high strength at higher temperatures, good corrosion resistance and high thermal conductivity, molybdenum is widely used in a variety of industrial processes, such as the production of metal alloys [4]. A risk of toxic exposure of workers in these industrial fields exists and environmental contamination near the industrial plants may be possible [5]. Molybdenum occurs principally in the hexavalent oxidation state as molybdate (MoO_4^{2-}) ions, which form condensed species in acid media [6]. In strongly acidic solutions, molybdenyl cations (MoO_2^{2+}) are present [7]. The concentration of molybdenum in seawater was reported in the range of 6–20 μg L^{-1} [8] and in mineral waters in the range of 0.25–1.0 μg L^{-1} [9], far below the drinking water guidelines (70 μg/L) [10].

Molybdenum naturally occurs in various ores, especially molybdenite (MoS_2) [11,12]. Most Mo compounds have very low solubility in water [13]; however, they are easily oxidized to produce the more soluble molybdate ion (MoO_4^{2-}), which can be stable in the absence of a reducing agent.

Water soluble molybdate anions cause an environmental problem if their concentration exceeds 5 ppm [14,15]. Molybdenum in soils is primarily in the oxoanion form and is chemisorbed by iron oxides, noncrystalline aluminosilicates, organic matter, and to a lesser extent, by layer silicate clays [11]. Under reducing conditions, molybdenum is easily bioaccessible by formation of soluble thiomolybdates, e.g. MoS_4^{2-} and $MoO_2S_2^{2-}$. Phosphate as well as organic acids additions to soil may release MoO_4^{2-} from binding sites [5].

Pollution by molybdate oxoanions in groundwater represents a serious issue in the field of drinking water obtained from wells [16]. For example, Mo is present in 32.7% of surface water samples from 15 major river basins in the USA, at concentrations ranging from 2 to 1500 μg L^{-1} (mean 60 μg L^{-1}). In addition, elevated Mo concentrations are reported in many mine wastes and mill tailings from North America where concentrations range from a few mg L^{-1} up to 800 mg L^{-1} [17].

Therefore, the search for suitable methods for groundwater/wastewater treatment against toxic oxoanions becomes very challenging. Coprecipitation [18] and reverse osmosis [19] are methods used for these treatments but they need various and complicated equipments and reagents. Simple sorption techniques have also been reported for the removal of molybdate from aqueous solution using different sorbents like $ZnCl_2$ activated coir pith carbon [12], pyrite [20], carbon cloth [21], natrolite and clinoptoliterich tuffs [22], orange peel [23], nano-ball allophone [24], γ-Al_2O_3 [25], magnetic chitosan resins [26], goethite [27], hematite [28], and modified bentonite [29].

The aim of this study is to evaluate Mo^{VI} sorption from aqueous solution in batch and column system using green seaweed biomass as sorbent. The sorbent was selected because of its natural abundance and low cost of obtaining in countries near the seas and the multiple functional groups present in its surface capable of binding Mo^{VI} species. These characteristics make this sorbent a better choice for being employed in treatment of Mo^{VI} contaminated waters. In fact, no other studies employing seaweeds in treatment of Mo^{VI} contaminated waters were reported. The sorption process has been investigated modifying different experimental parameters like pH, sorbent dosage, contact time and temperature. The competition of different anions onto Mo^{VI} sorption was also studied. The evaluation of sorption equilibrium and dynamics characteristics was done by using theoretical models in order to design and control the sorption process units. For that reason, equilibrium sorption data were applied to Langmuir, Freundlich and Dubinin–Radushkevich sorption models. Particle diffusion simple first order and pseudo first order rate equations were used to describe sorption kinetics. Activation energy, mean free sorption energy, and thermodynamic parameters like $\Delta G°$, $\Delta H°$ and $\Delta S°$ were also calculated. In addition, Mo^{VI} sorption was examined by FT-IR (Fourier transformed-Infrared spectroscopy), Scanning electronic microscopy (SEM) and Energy Dispersive X-ray Analysis (EDAX). Finally, green seaweed has been employed for removal of Mo^{VI} in a fixed-bed column. Some common theoretical models have been applied to fit the breakthrough curves.

2. Materials and methods

All chemicals used were of analytical reagent grade and were used without further purification. All solutions and seaweed suspensions were prepared using Milli-Q water. Mo^{VI} solutions of different concentrations were prepared by dissolving the proper amount of $Na_2MoO_4{\cdot}2H_2O$ (Sigma, p.a.) in water.

2.1. Biomass and pretreatment

Spongomorpha pacifica was collected at Puerto Madryn, Rio Negro, Argentina. The seaweed was carefully washed with mono distillate and Milli-Q water to remove salts, sand and microorganisms, which may interfere with the obtained results. Then, the material was dried in an oven at 40 °C for 24 h, crushed in a lab mill and sieved to obtain fine particles (0.5 < size < 1.2 mm). The resulting material was stored in a dry environment at room temperature. For determining the pH value at point of zero charge (pHpzc), 0.10 g of biomass was put into contact with 0.10 M $NaNO_3$ solution with different pH values (1.6–7.0). The suspensions were agitated for 24 h (250 rpm). The change of pH (ΔpH) was calculated as a difference between the initial pH and the equilibrium pH values. The pHpzc was identified as the initial pH with minimum ΔpH [30].

2.2. S. pacifica fixed in agar

A predetermined amount of seaweed biomass (size < 0.5 mm) and 10.0 ml of agar solution (20.0 g L^{-1}) previously heated, were added in a beaker. The suspension was mixed and transferred to a Petri dish of known mass and dimensions. Once the seaweed/agar suspension solidified, the matrix obtained was cut into 0.5 cm × 0.5 cm squares, which were stored in Milli-Q water in the refrigerator for later use.

2.3. Experimental design strategy. Screening design

In many cases there may be a lot of factors that seems to be important, but in reality only a few of them control the response in a significant way. The primary goal of screening designs is to identify the few factors or key variables that influence the response [31]. It is necessary to reduce the number of experiments and save time and cost. For this reason, a full 2^3 factorial design was performed. The factors considered were pH of solution, sorbent mass (m), and contact time (t). Table 1 shows the factors and their levels.

Table 1
Independent variables and their levels used for 2^3 factorial design.[a]

Variables	Symbol	Range and levels	
		−1	+1
Sorbent dosage (g L^{-1})	m	2	20
Contact time (min)	t	5	120
pH	pH	1	6

[a] $[MoO_4^{2-}]_0$ = 3.36 mM; batch volume = 10.0 mL; T = 20 °C.

The design also has three replicates at the center point, allowing us to check curvature in the response surface model [32,33].

2.4. Response surface design

The response surface approach is desirable to find a mathematical model capable of predicting the response. The optimized model was obtained by using the Central Composite Design (CCD) [34]. To do this, one should measure the response at some points of the working domain. The selection of these experimental points needs prior knowledge and should be done carefully to map the experimental domain correctly. Through running CCD, a regression model was fitted to the response (mg MoO_4^{2-} sorbed/g biomass). Such tests as lack of fit, analysis of variances (ANOVA), analysis of residuals distribution, over-fitting test, and coefficient of determination (R^2) were used to check the adequacy of the model [31,35]. All of the statistical and mathematical calculations were done by using Design Expert V. 7.0 software. Optimal conditions for sorption can be obtained by a visual or mathematical technique and compare theoretical and experimental responses, when a suitable model has been found.

2.5. Metal sorption experiments

The sorbent was suspended in solutions containing Mo^{VI} whose concentrations were set according to experimental design methodology. The seaweed dose in the solution was in the range of 2.0 ± 0.2 g L^{-1}. The seaweed/metal suspension was gently agitated (75 rpm) at controlled temperature. The pH of the solution was adjusted to the desired value by adding H_2SO_4 1.0 M. After a determined time, samples were taken from the solutions, and the Mo^{VI} concentration in the supernatants was determined spectrophotometrically at 400 nm by using a double-beam UV–vis spectrophotometer (JASCO V-550 model) after complexation with catechol in basic medium [36].

Kinetic studies were carried out in a glass beaker with magnetic stirring at three temperatures (20, 30 and 40 °C). 0.020 g of biomass was added to 10.0 mL of Mo^{VI} solution and keeping the suspension at constant pH throughout the experiment (pH 2.0). The assays were carried out at three different Mo^{VI} concentrations (0.010; 0.015 and 0.020 M). Samples (100 μL) of supernatant were taken at suitable time intervals and then analyzed for Mo^{VI} concentration. Metal uptake at different adsorbent- solution contact times (q, mg g^{-1}) was calculated using the general definition, Eq. (1):

$$q = \frac{C_0 V_0 - C_t V_t}{m} \tag{1}$$

where C_0 and C_t are the MoO_4^{2-} concentrations in solution (mg L^{-1}) at time 0 and t, respectively, V_0 and V_t are the solution volumes (L) at time 0 and t, respectively, and m is the mass of the sorbent used (g).

Isotherm assays were carried out at three different temperature values (20, 40 and 60 °C) by varying the initial concentration of metal from 0.10 to 50.0 mg L^{-1} (sorbent dosage = 2.0 g L^{-1}, pH 2.0). After reaching equilibrium, a sample (100 μL) of supernatant was taken and then analyzed for Mo^{VI} concentration. Eq. (1) was used to calculate the sorption capacity of the sorbent, q_e.

2.6. Column experiments

The sorption of Mo^{VI} by *S. pacifica* packed in glass columns of 15 cm long and 1.4 cm of internal diameter were studied. At the bottom end of the column a fiberglass cap was placed to avoid seaweed particles losses. The columns were filled, and later compacted by gravity with *S. pacifica* fixed in agar, keeping constant the package density. The top of the column was connected to a peristaltic pump (Gilson) using a silicone tube to obtain a constant steady downward flow of 0.60 mL min^{-1}. Solutions of a known concentration of sodium molybdate were pumped through the columns at constant pH 2.0 and room temperature. Samples of 1.0 mL were collected at time intervals to assess the residual concentration of metals and to determine the retained amount of metal. The aqueous solutions containing the pollutants flowed from beginning to end of the column passing through the packed sorbent material. The sorption capacity of Mo^{VI} was determined from Eq. (2).

$$q = \frac{C_{in} Q}{1000\, m} \int_0^t \left(1 - \frac{C_{out}}{C_{in}}\right) dt \tag{2}$$

where q is the mass of metal sorbed (mg MoO_4^{2-} g biomass^{-1}); C_{in} is the inlet solution concentration (mg L^{-1}); C_{out} the outlet solution concentration (mg L^{-1}); m is the amount of biomass in the column (g) and Q is the volumetric flow (mL min^{-1}).

In most industrial wastewater treatment units, a continuous mode of operation is preferred. The column bed performance is usually described through the concept of a breakthrough curve, which is obtained by plotting C/C_0 against time (C and C_0 are concentration of the outlet and inlet solutions at the column, respectively). Breakthrough and saturation time, sorption yield (%), and MoO_4^{2-} ions uptake are relevant parameters that can be obtained from the breakthrough curve as follows:

Breakthrough time (t_b, min) is considered on the basis of the effluent discharge limit for MoO_4^{2-} ions. So, the breakthrough time was obtained for an effluent MoO_4^{2-} concentration of 5.0 mg L^{-1}. Saturation time (t_{sat}, min) is usually considered when the effluent concentration remains close to influent concentration for a long period (corresponding to $C/C_0 = 0.95$). The uptake capacity (q_{ads}, mg g^{-1}) is obtained by dividing the quantity of MoO_4^{2-} sorbed (m_{ads}) by the sorbent mass (m) (Eq. (3)).

$$q_{ads} = \frac{m_{ads}}{m} \tag{3}$$

where the total quantity of MoO_4^{2-} sorbed by the biomass in the column (m_{ads}, mg) is calculated by subtraction of the quantity of MoO_4^{2-} joined at the column (m_{inlet}, mg) and the quantity of MoO_4^{2-} going out the column (m_{outlet}, mg) (Eqs. 4–6).

$$m_{inlet} = C_0\, Q\, t_{sat} \tag{4}$$

$$m_{outlet} = Q \int_0^{tsat} (C_0 - C) dt \tag{5}$$

$$m_{ads} = m_{inlet} - m_{outlet} \tag{6}$$

Various simple mathematical models have been developed to describe and possibly predict the dynamic behavior of the column bed. Thomas model is one of the most general and widely used models in column performance theory. Thomas solution assumes Langmuir model of sorption–desorption, and no axial dispersion is derived with the sorption that the rate driving force obeys pseudo-second order reversible reaction kinetics [37].

The expression of Thomas model is given in Eq. (7).

$$\frac{C_t}{C_0} = \frac{1}{1 + \exp\left(\frac{(q_{Th} m - C_0 v t) k_{Th}}{v}\right)} \tag{7}$$

where k_{Th} (mL min^{-1} mg^{-1}) is Thomas rate constant, q_{Th} (mg kg^{-1}) is the theoretical saturated sorption capacity in Thomas model, v (mL min^{-1}) is the flow rate of the effluent, m (kg) is the mass of the sorbent, C_0 (mg L^{-1}) is the influent MoO_4^{2-} concentration, C_t (mg L^{-1}) is the effluent MoO_4^{2-} concentration at time t (min). The value of C_t/C_0 is the ratio of effluent and influent MoO_4^{2-} concentrations at certain time. The kinetic coefficient k_{Th} and the sorption capacity of the column q_{Th} can be determined from a plot of C_t/C_0 against t at a given flow rate using non-linear regression.

Modified dose–response model minimized the error that results from use of the Thomas model, especially with lower and higher breakthrough curve times [38]. Its equation can be described as shown in Eq. (8).

$$\frac{C_t}{C_0} = 1 - \frac{1}{1 + \left(\frac{vt}{b}\right)^a} \quad (8)$$

where v (mL min^{-1}) is the flow rate of the effluent. Parameters a and b comes from the modified dose–response model.

In order to provide information about the stability of the sorbent, DOC (dissolved organic carbon) concentrations in the leachates were measured in column effluents. DOC concentrations were analyzed in a TOC-V_{WS} (SHIMADZU). Effluent samples were filtered through a 0.2 mm membrane prior to the analysis. DOC concentrations in the leachates were less than 0.01 mg mL^{-1}, indicating that sorbent packed in the column is very stable.

2.7. FTIR, SEM and EDAX analysis

FTIR spectroscopy (Perkin Elmer FT-IR Spectrum One spectrophotometer) was done to identify the chemical functional groups present on *S. Pacifica* and Mo^{VI}-loaded biomass. IR absorbance data were obtained for wavenumbers in the range of 400–4000 cm^{-1} employing the KBr dilution technique (1.5%, w/w). The surface structure of the seaweed before and after Mo^{VI} sorption was analyzed by scanning electron microscopy and the presence of Mo sorbed at the surface was confirmed by EDAX microanalysis (SEM Fei model QUANTA 200F, EDS EDAX with Si/Li detector). Experiments were made in Low Vacuum mode (LV 0.20–0.40 mbar chamber pressure), work distance (WD) 10 mm–12 mm. Image collections were obtained on non-coated samples at HV 5–10 kV, under low vacuum conditions. For semi quantitative EDAX analysis of Mo, HV of 30 kV was employed. The SEM images and EDAX analysis were performed at LM CCT Rosario Laboratory.

3. Results and discussion

3.1. FTIR analysis

In order to determine which functional groups are responsible for molybdate ions uptake, FTIR spectra of the sorbent, before and after MoO_4^{2-} uptake, were recorded. The spectra of sorbent were measured in the range of 400–4000 cm^{-1}. The spectra show a number of absorption peaks, indicating the complex nature of the material studied (see Fig. 1).

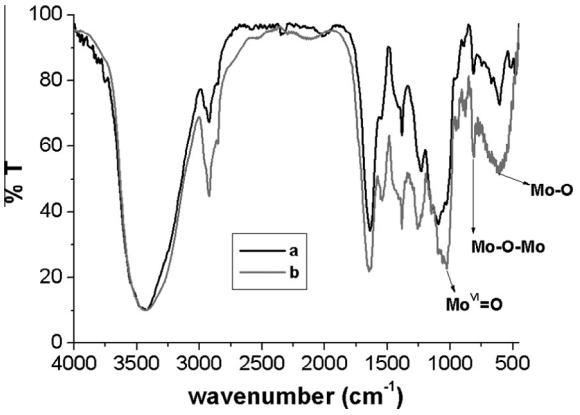

Fig. 1. FTIR spectra of (a) native green alga and (b) MoO_4^{2-} loaded green alga.

The FTIR spectrum of green seaweed exhibits a broad peak at 3438 cm^{-1}, which corresponds to the O–H stretching vibrations of cellulose, pectin, absorbed water, hemicellulose, and lignin. The OH stretching vibrations occur within a broad range of frequencies, indicating the presence of free hydroxyl groups and bonded OH bands of carboxylic acids [39–41]. The band at 2924 cm^{-1} indicates symmetric or asymmetric CH stretching vibration of aliphatic acids. The peak at 2854 cm^{-1} was the symmetric stretching vibration of CH_2 due to CH bonds of aliphatic acids. Bands around 1639 cm^{-1} correspond to esterified carboxyl groups [42]. The peak at 1384 cm^{-1} may be assigned to symmetric stretching of —COO^-. The band observed at 1094 cm^{-1} was assigned to C—O stretching of alcohols [43]. When the biomass was loaded with MoO_4^{2-}, differences in the positions of the absorbance peaks and new peaks appeared. Stretching mode corresponding to Mo=O was observed at 1026 cm^{-1} and vibrations corresponding to Mo—O appeared at 610 cm^{-1}. The peak at 810 cm^{-1} was assigned to Mo—O—Mo [44], and it suggests that formation of polynuclear species occurs at the surface of the adsorbent. No vibrations corresponding to Mo—N was observed (ν_{st} Mo—N: 470 cm^{-1}), suggesting that active surface sites are oxygenated groups. The peak at 3419 cm^{-1} assigned to O—H stretching was shifted and broadened and the C—O vibration was strengthen suggesting that hydroxyl groups are involved in the coordination of molybdate ions at the surface of the green seaweed. Antisymmetric stretching of —COO^- was shifted at 1646 cm^{-1} and symmetric stretching of —COO^- was shifted at 1385 cm^{-1}. These modifications in the stretching modes of —COO^- after treatment with MoO_4^{2-} suggest that deprotonated carboxylic groups are involved in the coordination of molybdate ions onto the surface of green seaweed.

3.2. Surface characterization

Scanning electron microscope (SEM) images were used for *S. pacifica* surface analysis (see Fig. S1, Supplementary Material).

SEM images were taken by applying 5–10 kV voltage with different magnification times. Fig. S1A (Supplementary Material) demonstrates the amorphous superficial structure of the seaweed biomass surface. The surface present fold-like structures in a random arrangement on the surface. After Mo^{VI} sorption, surface displayed an apparent flattening (see Fig. S1C Supplementary Material). The results obtained in this study are in agreement with the work of Murphy et al. [45], who observed changes in surface morphology of seaweeds after treatment with Cr^{III} and Cr^{VI}. Changes in surface morphology were due to an exchange of the Mo^{VI} ions with alkali metals causing relaxation of the biomass structures thus leading to an apparent flattening of the seaweed surface. Green seaweed contains cellulose in their inner cell wall with the outer cell wall consisting of an amorphous embedding matrix. This matrix is predominately pectin and mucilage [45]. Changes in the surface morphology after Mo^{VI} sorption indicates some rearrangement of surface polymer chains. Also some inclusions appeared as a consequence of polynuclear Mo^{VI} aggregates (see Fig. S1D, Supplementary Material).

EDAX analysis of Mo-loaded green seaweed performed at 30 kV voltage, showed a characteristic signal of Mo at 17.3 keV (see Fig. S2, Supplementary Materials), demonstrating that Mo was present in the surface of green seaweed.

3.3. Evaluation of the most significant constituents affecting molybdate sorption

Preliminary identification of significant factors was done by using a full 2^3 factorial design with three repeats at the center point (see Table S1, Supplementary Material).

Only pH and sorbent dose are significant factors ($P < 0.05$) and sorbent dose has the greatest effect. The negative sign means increasing its level from low to high decreases the removal percentage.

3.4. Improvement with central composite design

In order to improve molybdate sorption, the central composite design was applied to select experiments (see Table S2, Supplementary Material).

Data were analyzed using multiple regression analysis. The relationship between molybdate sorption (Y) and the test variables in coded factors was:

$$Y = 11.91 - 7.43\,A - 8.38\,B + 4.90\,A^2 + 3.45\,B^2 + 4.07\,AB \quad (9)$$

To validate the regression coefficient, analysis of variance was performed. The model F-value of 22.51 implies that the model is significant. Values of Prob > F less than 0.0500 indicate that the model terms are significant (see Table S3, Supplementary Material). R^2 of this model is 0.9575, which is considered as having a high correlation. Therefore, it is reasonable to apply the model to analyze the trends of the responses.

The 3D surface plot was the graphical representation of the regression in Eq. (9), from which the molybdate sorption, at different pH and adsorbent doses values can be predicted (see Fig. S3, Supplementary Material).

The obtained results indicate that the maximum value of molybdate sorption was obtained at pH 2.0 and sorbent dose = 2.0 g L^{-1}. At pH 2.0, the predominant Mo^{VI} specie is $H_3Mo_7O_{24}^{3-}$ (See Fig. S4, Supplementary Material), as calculated by HYDRA and MEDUSA Programs [46]. The point of zero charge (pHzpc) is the pH value of the solution, where the surface charge density is equal to zero, i.e. the number of positively charged centers is equal to the number of negatively charged centers. If pH < pHzpc the sorbent surface area is positively charged, and if pH > pHzpc, the sorbent surface area is negatively charged [47]. The point of zero charge (pHzpc) represents the value at which the curve ΔpH = f (pHi) intersects pHi axis (see Fig. S5, Supplementary Material).

The corresponding pHzpc, is 5.5. It means that at values pH < 5.5, the surface area of the green seaweed is positively charged and, at pH 2 strongly attracts the negatively charged heptamolybdate species.

In order to verify the improved effect by statistically designed experiments, a reaction with recipes at optimal conditions was performed. The experimental q value obtained (46,100 mg MoO_4^{2-}/kg biomass) was in agreement with the calculated value using Eq. (9) (46,220 mg MoO_4^{2-}/kg biomass). This similarity between the predicted and observed result reflects the accuracy and applicability of the central composite design as an extremely powerful method for optimizing the molybdate adsorption onto algae surface.

3.5. Kinetic studies

The prediction of sorption rate gives important information for designing continuous bed sorption systems. Information on the kinetics of solute uptake is required for optimum operating conditions for a continuous bed reactor [48]. The kinetics of the sorption data were modeled using a pseudo first-order kinetic model. Initially, it must be assumed that the sorption follows the Langmuir model, which agrees with chemisorption as being the rate controlling mechanism and this has been confirmed in the next section. The rate of the pseudo first-order reaction may be dependent on the amount of metal ion on the surface of the sorbent and the amount of metal ion sorbed at equilibrium. The pseudo first-order kinetic model was expressed as shown in Eq. (10):

$$\frac{dq_t}{dt} = k_{ads}(q_e - q_t) \quad (10)$$

where k_{ads} (min^{-1}) is the first-order-rate constant of sorption, q_e (mg kg^{-1}) is the molybdate amount sorbed on the sorbent at equilibrium time, and q_t (mg kg^{-1}) is the molybdate amount sorbed at time t [49].

After integration, by applying the following boundary conditions:

$q_t = 0$ at $t = 0$ and $q_t = q_t$ at $t = t$; Eq. (10) becomes:

$$\ln(q_e - q_t) = \ln(q_e) - k_{ads}\,t \quad (11)$$

Fig. 2 showed the kinetic data and best fit employing Eq. (5) working at three different initial concentration of MoO_4^{2-}.

As it saw in Fig. 2, k_{ads} was independent of $[MoO_4^{2-}]_0$ confirming the first order dependence.

The validity of the model was checked by the fitness of the straight line (R^2) as well as the consistence between experimental and calculated values of q_e.

Bhattacharya and Venkobachar [50] presented a simple first order reversible kinetic model (Eq. (12)), based on solution concentration for the sorption of Cd^{II} from liquid phase onto both Giridih coal and crushed coconut shell, as a reversible reaction with an equilibrium being established between two liquid and solid phases.

$$\ln(1 - U_{(t)}) = -kt \quad (12)$$

in which k is the overall first order rate constant (min^{-1}) and $U_{(t)} = \frac{[Mo^{VI}]_0 - [Mo^{VI}]_t}{[Mo^{VI}]_0 - [Mo^{VI}]_e}$.

Comparing both models, pseudo first order kinetic model has higher r^2 (higher than 0.992) and a better description of the kinetic data expressed as a consistence between experimental and calculated values of q_e (see Table 2). Simple first order kinetic model has r^2 values around 0.985 and lower description of kinetic data because at zero time, it is expected that the function equals to zero, and Fig. S6 (Supplementary Material) showed that y-intercept were not equals to zero.

Most sorption reactions take place through multistep mechanism comprising (i) external film diffusion, (ii) intraparticle diffusion and (iii) interaction between sorbate and active site. The first step is excluded by shaking the solution. So the rate determining step is one of the two other steps. To know if the intraparticle diffusion is the rate determining step or not, the uptake/time data (see Fig. S7) was treated according to Weber and Morris diffusion model [51] (Eq. (13)).

$$q_t = k_{id}\,t^{1/2} \quad (13)$$

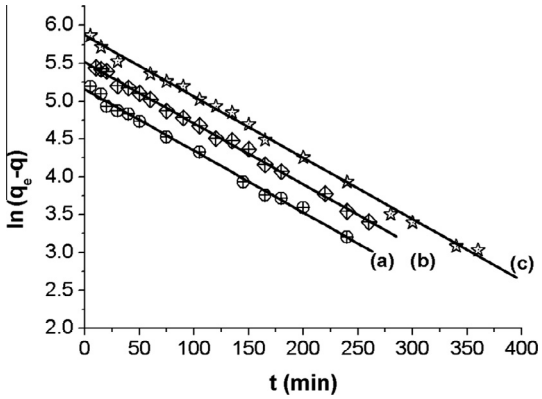

Fig. 2. Kinetic data and best fit employing pseudo first-order kinetic model. Biomass doses = 2.0 g L^{-1}; T = 20 °C; pH = 2.0; (a) $[MoO_4^{2-}]_0$ = 0.010 M; (b) $[MoO_4^{2-}]_0$ = 0.015 M and (c) $[MoO_4^{2-}]_0$ = 0.020 M.

Table 2
Characteristic parameters of the different kinetic models and coefficients of determination (r^2).[a]

T (°C)	20	30[d]	40[d]
Pseudo-first order			
q_e (mg kg^{-1})	$1.742 \times 10^5 \pm 200$[b] $2.472 \times 10^5 \pm 300$[c] $3.542 \times 10^5 \pm 400$[d]	$2.846 \times 10^5 \pm 300$	$2.281 \times 10^5 \pm 200$
k_{ads} (min^{-1}) $\times 10^3$	8.1 ± 0.2[b] 8.1 ± 0.1[c] 8.1 ± 0.1[d]	12.2 ± 0.3	17.1 ± 0.6
r^2	0.9949[b] 0.9970[c] 0.9966[d]	0.9958	0.9923
Simple first order			
k (min^{-1}) $\times 10^3$	8.0 ± 0.6[b] 7.5 ± 0.8[c] 7.9 ± 0.4[d]	10.2 ± 0.6	16.7 ± 0.8
r^2	0.9829[b] 0.9759[c] 0.9888[d]	0.9856	0.9815
Intraparticle diffusion			
k_{id} (mg kg^{-1} min$^{-0.5}$)	$1.71 \times 10^4 \pm 700$[b] $2.19 \times 10^4 \pm 700$[c] $2.81 \times 10^4 \pm 900$[d]	$2.85 \times 10^4 \pm 700$	$2.9 \times 10^4 \pm 1000$
r^2	0.6599[b] 0.7349[c] 0.7253[d]	0.7895	0.7991

[a] Biomass doses = 2.0 g L^{-1}; pH = 2.0.
[b] $[MoO_4^{2-}]_0$ = 0.010 M.
[c] $[MoO_4^{2-}]_0$ = 0.015 M.
[d] $[MoO_4^{2-}]_0$ = 0.020 M.

where k_{id} (mg kg^{-1} min$^{-1/2}$) is the intraparticle rate constant and can be obtained from non-linear curve fit of kinetic data.

As can be seen from Fig. S7 inset, the sorption was controlled by three different stages: the first sharper portion being a rapid external surface sorption, the second linear portion being a gradual sorption where intraparticle diffusion is the rate limiting factor, and the final portion being final equilibrium stage due to low concentration of molybdate ions in solution phase as well as less number of available sorption sites. It is clear that intraparticle diffusion is not the only rate determining step as the second portions of plots of q_t versus $t^{1/2}$ did not have zero intercept [52]. For the sorption of molybdate ions onto seaweed surface, the linear plots of Eq. (10) have a good correlation of the data as shown in Fig. 2.

The correlation coefficients, r^2, for the pseudo-first order kinetic model are much greater than the intraparticle diffusion coefficients for the sorption/reaction of molybdate ions onto biomass surface, strongly suggesting a chemical reaction mechanism. Table 2 resumes the values of k_{ads}, k, k_{id} and correlation coefficients obtained at three different temperatures.

Numerical value for activation energy of soption process was obtained by plotting experimental data for rate constants at different temperatures. From the logarithmic form of the Arrhenius equation a plot of $\ln k_{ads}$ versus $1/T$ yields a slope equal to $-E_a/R$. Since the sorption rates of the molybdate ions increased with temperature, the slope of Arrhenius plot gives a negative value and the activation energy is found to be positive (see Fig. S8, Supplementary Material).

E_a afforded a value of 28.52 kJ mol^{-1}. For biological systems, the reported activation energies in the literature generally change over the range 8.4–83.7 kJ mol^{-1} [53]. Two main types of sorption may occur: physical and chemical sorption. In physical sorption, equilibrium between the sorbent surface and the sorbate is usually rapidly attained and easily reversible, because the energy requirements are small. Activation energy for physical sorption is usually no more than 4.184 kJ mol^{-1}, since the forces involved in physical sorption are weak [54], meanwhile for chemisorptions values of E_a higher than 8.4 kJ mol^{-1} are expected. The value of E_a obtained is in agreement with a chemisorption mechanism.

3.6. Sorption isotherms

The equilibrium between the sorbate immobilized on the active sites of a sorbent and the sorbate remaining in the aqueous phase is usually presented by sorption isotherms. In order to describe the uptake of molybdate ions by green seaweed biomass, the isotherms data were analyzed using three models, Langmuir, Freundlich and Dubinin–Radushkevich (D–R).

Langmuir isotherm is given by Eq. (14) [55]:

$$q_e = \frac{q_m K_L C_e}{1 + K_L C_e} \tag{14}$$

where C_e is the equilibrium concentration of metal ions (mg L^{-1}), q_e is the amount of metal ions required to form a monolayer onto the sorbent surface (mg kg^{-1}), K_L is the Langmuir equilibrium constant. The essential feature of the Langmuir isotherm can be expressed by means of a separation factor or equilibrium parameter, R_L, is calculated using Eq. (15) [56].

$$R_L = \frac{1}{1 + K_L C_0} \tag{15}$$

where C_0 is the highest MoO_4^{2-} concentration (mol L^{-1}). As the R_L values lie between 0 and 1, the sorption process is favorable.

Freundlich sorption isotherm is given by Eq. (16) [57].

$$q_e = K_F C_e^{1/n} \tag{16}$$

where C_e is the equilibrium concentration of metal ions (mg L^{-1}), q_e is the amount of metal ions required for forming a monolayer onto the sorbent surface (mg kg^{-1}), K_F and $1/n$ are the Freundlich equilibrium constant and the coefficient of heterogeneity in the Freundlich sorption isotherm equation.

The Dubinin–Radushkevich (D–R) sorption isotherm is given by Eq. (17) [58].

$$q_e = q_m e^{-\beta\varepsilon^2} \quad (17)$$

where β is a constant related to the mean free energy of sorption ($mol^2\ J^{-2}$), q_m the theoretical saturation capacity, and ε is the Polanyi potential, which is equal to $RT\ \ln(1 + (1/C_e))$, where R (J mol^{-1} - K^{-1}) is the gas constant and T (K) is the absolute temperature.The constant β gives an idea about the mean free energy E (kJ mol^{-1}) of sorption and can be calculated using the relationship showed in Eq. (18) [59].

$$E = \frac{1}{(2\beta)^{1/2}} \quad (18)$$

E values give information about sorption mechanism as chemical ion-exchange or physical sorption. With the magnitude of E, between 8 and 16 kJ mol^{-1}, the sorption process follows chemical ion-exchange, while for the values of $E < 8$ kJmol^{-1}, the sorption process is of a physical nature. The numerical values of the mean free energy of sorption at three different temperatures and the various constants of the three models were calculated and were represented in Table 3.

E values were in the range 9–13 kJ mol^{-1}, indicating that the sorption process follows chemical ion-exchange. This result agrees with the conclusion obtained in Arrhenius plot.

By comparing the correlation coefficients, it can be concluded that Langmuir isotherm provides a good model for the sorption system, which is based on monolayer sorption onto surface containing finite number of identical sorption sites. The maximum sorption capacity decreases with increasing T, this result was previously found for others systems [60,61], and it is attributed to a loss of sorption sites due to degradation of the biomass with temperature. The value of the dimensionless parameter R_L indicates that the sorption is favorable ($0 < R_L < 1$). The E values lies between 8 and 16 kJ mol^{-1} as shown in Table 3, which suggests that sorption occurred by ion-exchange mechanism [62].

The comparison of sorption capacity of green seaweed biomass with that of various sorbents is shown in Table 4.

The green seaweed has a high sorption capacity as comparable with that of the other sorbents. Therefore, considering the low cost of this natural sorbent (waste), it can be used as an alternative material to minimize the concentration of MoO_4^{2-} ions in groundwater and wastewater.

The isotherm profiles of molybdate sorption at various T values are shown in Fig. 3. Experimental results are well represented by Langmuir isotherm at the three temperatures studied.

Table 4
Comparison between the sorption of MoO_4^{2-} ions by green seaweed and other sorbents reported in literature.

Sorbent	MoO_4^{2-} uptake (mg/kg)	Reference
Organo-bentonite	2.24×10^5	[28]
Goethite	2.59×10^4	[26]
Zr(IV)-orange peel gel	2.16×10^5	[22]
Fe(III)-orange peel gel	1.76×10^5	[22]
Ce(III)-orange peel gel	1.584×10^5	[22]
La(III)-orange peel gel	1.952×10^5	[22]
Magnetic chitosan resin	1.28×10^6	[25]
Hematite	1.039×10^4	[27]
Green seaweed	1.28×10^6	This work

3.7. Sorption thermodynamics

In engineering practice, values of thermodynamic parameters such as enthalpy change ($\Delta H°$), entropy change ($\Delta S°$) and free energy change ($\Delta G°$) must be taken into consideration in order to determine the spontaneity of a process.

The sorption free energy change, $\Delta G°$, is known by Eq. (19).

$$\Delta G° = -RT\ \ln\ K_L \quad (19)$$

where K_L is the Langmuir constant (L mol^{-1}), R is the universal gas constant (8.314 J mol^{-1} K^{-1}), and T is the temperature (K).

It is recognized that $\Delta G°$ is given as J mol^{-1} l, and so the equilibrium constant K_L in Eq. (19) has to be dimensionless [63,64]. The K_L constant is simply recalculated as dimensionless by multiplying it by 55.5 (mol H_2O L^{-1}).

Taking into account the last consideration, $\Delta G°$ value is expressed as shown in Eq. (20) [65].

$$\Delta G° = -RT\ \ln 55.5K_L \quad (20)$$

The heat of sorption of the sorbent, $\Delta H°$ (kJ mol^{-1}), and entropy $\Delta S°$ (J mol^{-1} K^{-1}) for the sorption process is given in Eq. (21):

$$\Delta G° = \Delta H° - T\Delta S° \quad (21)$$

For the determination of $\Delta H°$ and $\Delta S°$ the equation above can be written as shown in Eq. (22).

$$\ln 55.5K_L = \frac{\Delta S°}{R} - \frac{\Delta H°}{R}\frac{1}{T} \quad (22)$$

The obtained thermodynamic data are shown in Table 5.

The positive values of $\Delta S°$ and $\Delta H°$ obtained using Eq. (22), indicated an increase in randomness and the endothermic nature of the sorption processes. Therefore, increasing the solution temperature will enhance the binding potential at equilibrium [66,67].

Table 3
Characteristic parameters of the different isotherm models and coefficients of determination (r^2).

	T 20 °C	T 40 °C	T 60 °C
Langmuir			
q_m (mg kg^{-1})	$1.28 \times 10^6 \pm 1 \times 10^4$	$8.40 \times 10^5 \pm 2 \times 10^3$	$5.00 \times 10^5 \pm 1 \times 10^3$
K_L (L mg^{-1})	0.057 ± 0.006	0.12 ± 0.02	0.21 ± 0.02
R_L	0.260	0.154	0.091
r^2	0.9993	0.9934	0.9947
Freundlich			
K_F	87 ± 7	110 ± 8	103 ± 7
$1/n$	0.75 ± 0.04	0.61 ± 0.03	0.50 ± 0.03
r^2	0.9939	0.9897	0.9822
D–R			
q_m (mg kg^{-1})	$1.45 \times 10^6 \pm 5 \times 10^4$	$6.90 \times 10^5 \pm 6 \times 10^3$	$3.10 \times 10^5 \pm 2 \times 10^3$
β ($mol^2\ J^{-2}$) $\times 10^9$	6.1 ± 0.2	4.2 ± 0.2	3.1 ± 0.2
E (kJ mol^{-1})	9.05 ± 0.02	10.91 ± 0.03	12.70 ± 0.06
r^2	0.9963	0.9928	0.9897

Biomass doses 2.0 g L^{-1}; pH = 2.0; contact time: 6 h; $[MoO_4^{2-}]_0$ = 0.10–50.00 mg L^{-1}.

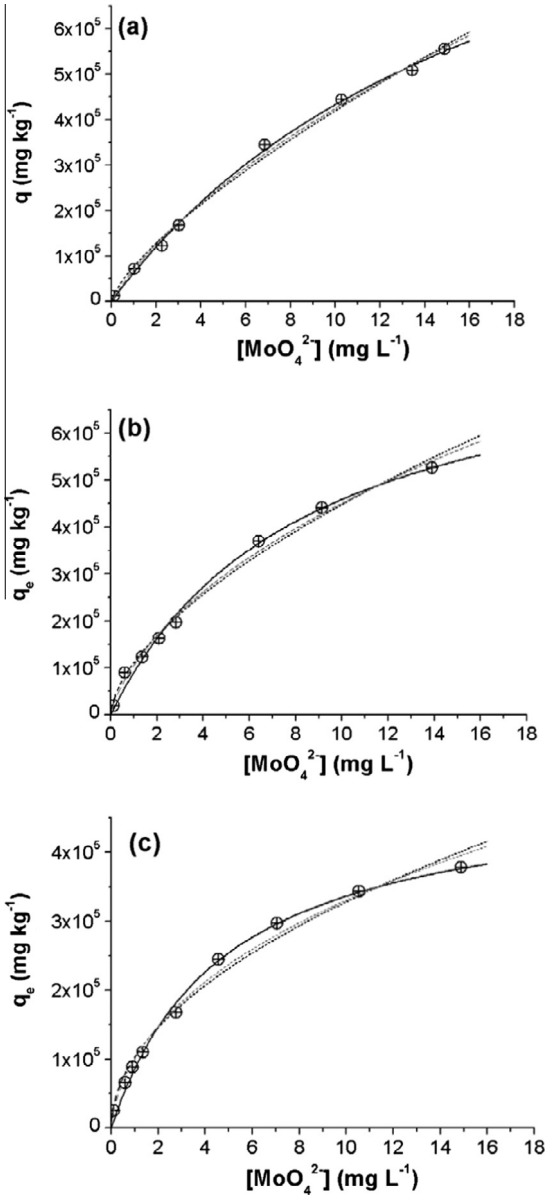

Fig. 3. Sorption isotherm of molybdate ions onto green seaweed. Biomass doses = 2.0 g L^{-1}; pH = 2.0; $[MoO_4^{2-}]_0$ = 0.10–50.00 mg L^{-1}; contact time 6 h. — Langmuir Model; --------- Freundlich Model; ---------- D–R Model. (a) 20 °C; (b) 40 °C and (c) 60 °C.

Table 5
Thermodynamic parameters of molybdate sorption by green seaweed.

Temperature (K)	$\Delta G°$ (kJ mol^{-1})	$\Delta H°$ (kJ mol^{-1})	$\Delta S°$ (J K^{-1} mol^{-1})
293	−32.02	+25.46	+196.2
313	−35.92		
333	−39.87		

The endothermic sorption processes imply that diffusion from bulk solution to sorbent boundary possibly will involve energy to overcome the interaction of water molecules with molybdate ions [68,69]. Positive $\Delta S°$ values also show that ion replacement reactions took place. The negative values of $\Delta G°$ show that the sorption processes were spontaneous in the temperature range studied.

3.8. Isosteric heat of sorption

Isosteric heats of sorption are key thermodynamic parameters in design of separation processes [70]. The heats can be strong and complex functions of sorbate loadings when the sorbent is energetically heterogeneous. Ignoring these characteristics in process design can lead to serious errors [71]. The heat of sorption determined for a constant amount of sorbed sorbate is known as the isosteric heat of sorption and is calculated using Clausius–Clapeyron equation [72] (Eq. (23)).

$$\frac{d\ln(C_e)}{dT} = -\frac{\Delta H_{st}}{RT^2} \tag{23}$$

For this purpose, plots of $\ln C_e$ versus T^{-1} were derived for different amounts of sorbed MoO_4^{2-} ions and ΔH_{st} values were calculated from the slope of these isosters (Fig. 4A). The ΔH_{st} values are shown in Fig. 4B as a function of surface loading (amount of MoO_4^{2-} sorbed, mg kg^{-1}).

The isosteric heat of sorption decreases with surface loading, indicating that the green seaweed has an energetically non-homogeneous surface. This decrease occurs because the high-interaction-energy sites are filled first [73].

3.9. Sorption mechanism

The real challenge in the field of metal sorption studies is to identify the mechanism of metal uptake by the sorbent. One of the mechanisms suggested to be involved in sorption is the ion exchange process between protons and/or light metals as counterions present in the biomass and heavy metal ions taken-up from the metal containing aqueous solution [74]. From kinetic studies at various temperatures we obtained an activation energy value (E_a) of 28.52 kJ mol^{-1}. Activation energy for physical sorption is usually no more than 4.184 kJ mol^{-1}, since the forces involved in physical sorption are weak [54], meanwhile for chemisorptions values of E_a higher than 8.4 kJ mol^{-1} are expected. The value of E_a obtained is in agreement with a chemisorption mechanism. From equilibrium studies, application of Dubinin–Radushkevich (D–R) model allowed us to calculate mean free energy of sorption (E). E values obtained were in the range 9–13 kJ mol^{-1}. With the magnitude of E, between 8 and 16 kJ mol^{-1}, the sorption process followed chemical ion-exchange. Equilibrium studies performed at various temperatures allowed us to determine a ΔS value of +196.2 J K^{-1} mol^{-1}. Positive $\Delta S°$ values showed that ion replacement reactions took place. No redox reaction took place, because no evidence of Mo^V species was found. Combining all these results we proposed in Scheme 1, a possible mechanism for molybdate uptake by green seaweed.

Presence of heptamolybdate ions were proposed based on IR evidence of stretching frequencies assigned to these species and because at working pH (pH = 2), $H_3Mo_7O_{24}^{3-}$ is the major Mo^{VI} specie present in solution (see Fig. S4, Supplementary Material). Binding at hydroxyl and carboxylic functional groups were proposed based on IR evidence (frequencies assigned for these functional groups were modified after Mo^{VI} uptake by green seaweed).

3.10. Continuous sorption studies

The experimental breakthrough curves at three different bed heights and those obtained for the Modified dose–response model are represented in Fig. 5.

The experimental breakthrough time (the position at C/C_0 = 0.05), saturation time (the position at C/C_0 = 0.95), and MoO_4^{2-} ions uptake (mg g^{-1}) obtained experimentally were tabulated in Table S4 (See Supplementary Material). Thomas and

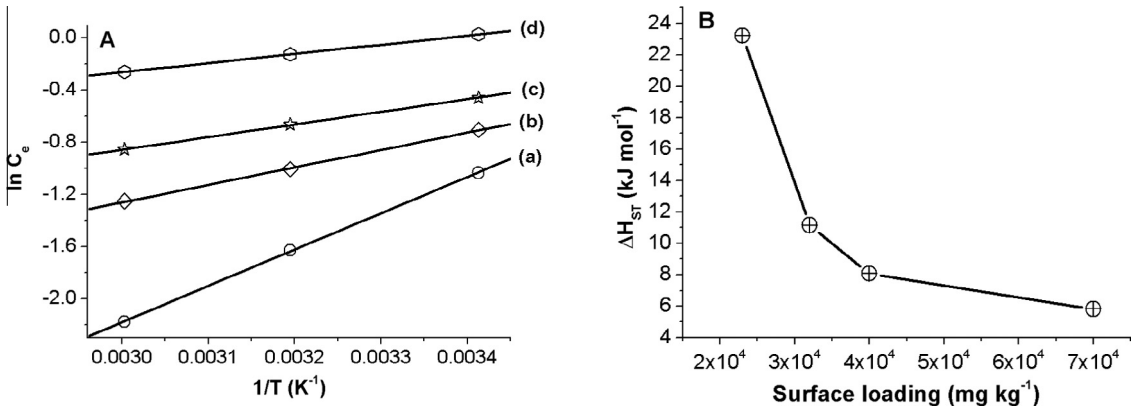

Fig. 4. A: Plots of $\ln C_e$ against $1/T$ for sorption of MoO_4^{2-} ions onto green seaweed. (a) 2.3×10^4 mg kg^{-1}; (b) 3.2×10^4 mg kg^{-1}; (c) 4.0×10^4 mg kg^{-1}; (d) 7.0×10^4 mg kg^{-1}. B: variation of isosteric heat of sorption with surface loading of MoO_4^{2-} ions onto green seaweed.

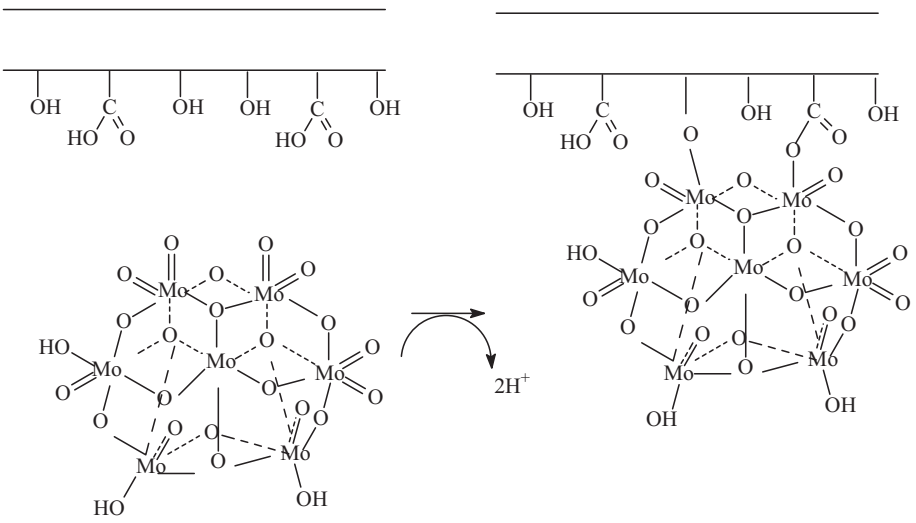

Scheme 1. Proposed mechanism for Mo^{VI} uptaking by green seaweed.

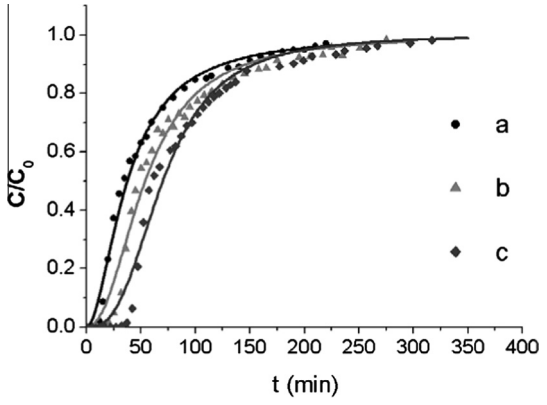

Fig. 5. Breakthrough curves and modified doses-response models for different bed heights. $C_0 = 80$ mg L^{-1} MoO_4^{2-}; $Q = 0.60$ mL min^{-1}; $T = 20$ °C; pH = 2.0. (a) $h = 3.0$ cm; (b) $h = 4.2$ cm and (c) $h = 6.0$ cm.

Modified dose–response parameters, and the correlation coefficients (r^2), are tabulated in Table 6.

The values of q_{Th} calculated from Thomas model, Eq. (7), were comparable to the q values calculated using Eq. (3). It was found that the Thomas model (r^2) range from 0.937 to 0.946 exhibited an adequate fit of the experimental data. In order to improve the fit of the experimental data, modified dose response model was applied. As shown in Table 6, values of r^2 increases to 0.981–0.991 allowing an excellent fit of the experimental breakthrough curves. The values of a and b increased with increasing the bed height. Similar behavior was reported by Albadarin et al. [75].

The breakthrough time, the saturation time and the biosorption yield increase as bed height increases since a higher bed depth results in a longer residence time of the solution in the column, allowing the MoO_4^{2-} ions to diffuse more deeply inside the sorbent, and so, all the above parameters increase.

3.11. Scale-up study

The bed depth service time (BDST) model predicts the relationship between the bed depth, Z (cm), and the operation time, t (min). This model assumes that the sorption rate is controlled by the surface reaction between the sorbate and the unused capacity of the sorbent [76].

Eq. (24) expresses a linear relationship between the bed depth and the service time:

$$t = \frac{N_0}{C_0 v} Z - \frac{1}{k_{BDST} C_0} \ln\left(\frac{C_0}{C_t} - 1\right) \quad (24)$$

Table 6
Different parameters for Thomas and modified dose–response models.

Z (cm)	Thomas model				Modified dose–response model			
	$k_{Th} \times 10^4$	$q_{Th} \times 10^6$	r^2	χ^2	a	b	r^2	χ^2
3.0	7.2 ± 0.3	0.322 ± 0.003	0.9432	0.00874	1.85 ± 0.02	22.7 ± 0.3	0.9913	0.0011
4.2	5.9 ± 0.6	0.326 ± 0.008	0.9375	0.00884	2.3 ± 0.2	31.7 ± 0.4	0.9810	0.00221
6.0	4.9 ± 0.3	0.331 ± 0.002	0.9464	0.00733	2.8 ± 0.1	42.8 ± 0.4	0.9808	0.00263

C_0 = 80 mg L^{-1} MoO_4^{2-}; Q = 0.60 mL min^{-1}; T = 20 °C; pH = 2.0.

Table 7
Different parameters for BDST model.

C_t/C_0%	$k_{BDST} \times 10^3$ (L mg^{-1} min^{-1})	N_0 (mg L^{-1})	r^2
5	2.3 ± 0.7	299.5 ± 0.4	0.9998
20	1.7 ± 0.8	302.6 ± 0.5	0.9994
50	–	327.6 ± 0.8	0.9985
80	1.8 ± 0.9	411.8 ± 0.9	0.9967

C_0 = 80 mg/L MoO_4^{2-}; v = 0.39 cm/min; T = 20 °C; pH = 2.0; z = 3.0; 4.2 and 6.0 cm.

where N_0 is the sorption capacity (mg L^{-1}), v is the fluid velocity (cm min^{-1}) determined from the calculation of volumetric flow rate over the bed section area, C_t is the outlet concentration at time t (mg L^{-1}) and k_{BDST} is the kinetic constant (L mg^{-1} min^{-1}). k_{BDST} and N_0 can be calculated from the linear and angular coefficient, respectively, from the graph of t as a function of Z at a given C_t/C_0 ratio (iso-concentration line).

Iso-concentration lines for molybdate ions removal in a fixed bed at C_t/C_0 = 5%, 20%, 50% and 80% were determined, (see Fig. S9, Supplementary Material).

Table 7 showed the k_{BDST} and N_0 parameters obtained for different C_t/C_0 ratios.

A consistent increase in slopes from 9.6 to 13.2 was observed for C_t/C_0 ratios of 5–80% and consequent increase in corresponding dynamic sorption capacity N_o from 299 to 411 mg L^{-1}. On the sorbent used, some active sites remain unoccupied by molybdate ions at lower C_t/C_0 ratio value, and hence the sorbent remained unsaturated. The dynamic sorption capacity in such low breakthrough condition was consequently bound to be lower than the full bed capacity of the sorbent [75]. The rate constant, k_{BDST}, characterized the rate of solute transfer from the fluid phase to the solid phase. It remains equals in the C_t/C_0 range employed.

To further check the validity of BDST model the breakthrough curve was inspected at 50%. At 50% breakthrough, C_o/C_t = 2, therefore reducing the logarithmic term of BDST equation to zero. Good correlation coefficient was obtained at 50% breakthrough suggesting the conformity of BDST model with sorption of Mo^{VI} by green seaweed. Therefore, the constants obtained using the BDST model could be used to predict the times at which the ratio C_t/C_0 equals 0.05–0.80 for other bed depths.

The critical bed depth, Z_0 is calculated by setting t = 0 and $C_t = C_b$.

It is given by Eq. (25).

$$Z_0 = \frac{v}{k_{BDST} N_0} \ln\left(\frac{C_0}{C_b} - 1\right) \quad (25)$$

The critical bed depth, Z_0 was determined to be 1.7 cm. This value is the minimum theoretical bed height of the sorbent that is sufficient such that the effluent concentration at t = 0 will not exceed the breakthrough concentration, C_b.

4. Conclusions

The present study reports the characteristic of molybdate ion sorption by a new sorbent (*S. pacifica* biomass). Principal aspects investigated for the purpose included optimization of the sorption process, kinetics and sorption isotherms modeling, FTIR, SEM and EDAX analysis, continuous sorption and scale- up studies. Optimization studies results in pH 2 and sorbent dose 2.0 g L^{-1} as optimal conditions for Mo^{VI} removal. FTIR analysis shows that hydroxyl and deprotonated carboxylic groups are involved in the coordination of molybdate species at the surface of green seaweed. SEM images shows that morphological changes occurs at the surface after Mo^{VI} sorption. The pseudo-first order kinetic and Langmuir sorption isotherm models were noted be fit to the experimental data. Q_{max} obtained was $1.28 \times 10^6 \pm 1 \times 10^4$ mg kg^{-1} and it was comparable with that of the other sorbents reported in literature. Activation parameters and mean free energies obtained with Dubinin–Radushkevich isotherm model confirm that the mechanism of sorption process was chemical sorption. Thermodynamic parameters demonstrate that the sorption process was spontaneous and endothermic. The driven force was entropic. The isosteric heat of sorption decreases with surface loading, indicating that *S. pacifica* has an energetically non-homogeneous surface. Experimental breakthrough curves were simulated by Thomas and modified dose–response models. The values of q_{Th} calculated from Thomas model, were comparable to the experimental q values. The breakthrough time, the saturation time and the sorption yield increase as bed height increases since a higher bed depth results in a longer residence time of the solution in the column, allowing the MoO_4^{2-} ions to diffuse more deeply inside the sorbent, and so, all the above parameters increase. Finally, the bed depth service time (BDST) model was employed to scale-up the continuous sorption experiments. The critical bed depth, Z_0 was determined to be 1.7 cm. This value is the minimum theoretical bed height of the sorbent that is sufficient such that the effluent concentration at t = 0 will not exceed the breakthrough concentration, C_b.

S. pacifica biomass results a good sorbent for Mo^{VI}. It has a better value of Q_{max} compared with sorbents derived from minerals such as hematite, goethite and organo-bentonite. The high value of Q_{max} and the low cost of this sorbent (approximately 1dollar per kg of green seaweed including pretreatment) makes this new sorbent a better choice for continuous treatment of effluents polluted with molybdate ions. For example, employing a column with a capacity of 100 dm^3 requires 27 kg of sorbent, and it cost 27 dollar for packing this column, making the process available at low costs.

Acknowledgments

We thank the National Research Council of Argentina (CONICET) PIP 0037 and National University of Rosario (UNR) BIO259 for financial support. We also thanks to the Argentine Technological Founding of Environmental and Social Development, for equipment donation. Bertoni thanks CONICET for providing a doctoral fellowship. We thanks also phD Patricia Blanes for donation of green seaweed.

Appendix A. Supplementary data

Supplementary data associated with this article can be found, in the online version, at http://dx.doi.org/10.1016/j.jcis.2015.01.033.

References

[1] R. Garg, M.K. Saini, N. Fahmi, R.V. Singh, Transit. Metal Chem. 31 (2006) 362–367.
[2] C. Neunhauserer, M. Berreck, H. Insam, Water Air Soil Pollut. 128 (2001) 85–96.
[3] S. Goldberg, S.M. Lesch, D.L. Suarez, Soil Sci. Soc. Am. J. 66 (2002) 1836–1842.
[4] H. Bei, S. Shim, E. George, M. Miller, E. Herbert, G. Pharr, Scr. Mater. 57 (2007) 397–400.
[5] K. Pyrzynska, Anal. Chim. Acta 590 (2007) 40–48.
[6] A.R. Ghiasvand, S. Shadabi, E. Mohagheghzadeh, P. Hashemi, Talanta 66 (2005) 912–916.
[7] G. Dodbibaa, T. Fujita, T. Kikuchib, J. Manjannaa, S. Matsuoa, H. Takahashic, K. Tohjic, Chem. Eng. J. 166 (2011) 496–503.
[8] H.C. dos Santos, M.G.A. Korn, S.L.C. Ferreira, Anal. Chim. Acta 426 (2001) 79–84.
[9] S.L.C. Ferreira, H.C. dos Santos, R.C. Campos, Talanta 61 (2003) 789–795.
[10] World Health Organisation (WHO), 2011. Molybdenum in Drinking-water. Geneva, Switzerland.
[11] R.L.F. Fontes, H.A. Coelho, Commun. Soil Sci. Plan. 36 (2005) 2367–2381.
[12] C. Namasivayam, D. Sangeetha, Bioresour. Technol. 97 (2006) 1194–1200.
[13] A. Vyskocil, C. Viau, J. Appl. Toxicol. 19 (1999) 185–192.
[14] A. Moret, J. Rubio, J. Miner. Eng. 16 (2003) 715–722.
[15] C. Wu, S. Lo, C. Lin, C. Kuoy, J. Colloid Interface Sci. 233 (2001) 259–264.
[16] P. Smedley, H. Nicolli, D. Macdonald, A. Barros, J. Tullio, Appl. Geochem. 17 (2002) 259–284.
[17] S. Das, M.J. Hendry, Appl. Geochem. 28 (2013) 194–201.
[18] R. Mamtaz, D. Bache, J. Water Supply: Res. Technol.-AQUA 50 (2001) 313–324.
[19] Y. Zhaoa, J. Taylor, S. Chellam, J. Membr. Sci. 263 (2005) 38–46.
[20] B.C. Bostick, S. Fendorf, G.R. Helz, Environ. Sci. Technol. 37 (2003) 285–291.
[21] A. Afkhami, B.E. Conway, J. Coll. Interface Sci. 251 (2002) 248–255.
[22] H. Faghihian, A. Malekpour, M.G. Maragheh, Int. J. Environ. Pollut. 18 (2002) 181–189.
[23] W. Shan, D. Fang, Z. Zhao, Y. Shuang, L. Ning, Z. Xing, Y. Xiong, Biomass Bioenergy 37 (2012) 289–297.
[24] E.A. Elhadi, N. Matsue, T. Henmi, Clay Sci. 11 (2001) 5–11.
[25] C.H. Wu, S.L. Lo, C.F. Lin, Colloids Surf. A: Physicochem. Eng. Aspects 166 (2000) 251–259.
[26] K. Elwakeel, A. Atia, A. Donia, Hydrometallurgy 97 (2009) 21–28.
[27] N. Xu, C. Christodoulatos, W. Braida, Chemosphere 62 (2006) 1726–1735.
[28] G. Dodbiba, T. Fujit, T. Kikuchi, J. Manjanna, S. Matsuo, H. Takahashi, K. Tohji, Chem. Eng. J. 166 (2011) 496–503.
[29] A. Atia, Appl. Clay Sci. 41 (2008) 73–84.
[30] H. Šillerova, M. Komarek, V. Chrastny, M. Novak, A. Vanek, O. Drabek, J. Colloid Interface Sci. 396 (2013) 227–233.
[31] J. Zolgharnein, A. Shahmoradi, J. Chem. Eng. Data 55 (2010) 5040–5049.
[32] D.L. Massart, B.G.M. Vandeginste, L.M.C. Buydens, S.D.E. Jong, P.J. Lewi, J. Smeyers Verbeke, Handbook of Chemometrics and Qualimetrics, Part A, Elsevier, Amsterdam, 2003.
[33] R.E. Bruns, I.S. Scarmino, B. de Barros Neto, Statistical Design-Chemometrics, first ed., Elsevier, Amsterdam, 2006.
[34] M.A. Bezerra, R.E.E. Santelli, P. Oliveira, L.S. Villar, L.A. Esclaleira, Talanta 76 (2008) 965–977.
[35] C. Huang, L. Chen, H. Yang, M. Li, T. Pan, J. Hazard. Mater. 241–242 (2012) 190–196.
[36] R. Soni, M. Bartusek, J. Inorg. Nucl. Chem. 33 (1971) 2557–2563.
[37] H.C. Thomas, J. Am. Chem. Soc. 66 (1944) 1664–1666.
[38] G. Yan, T. Viraraghavan, M. Chen, Adsorpt. Sci. Technol. 19 (2001) 25–43.
[39] C. Namasivayam, I.R. Kavitha, Microchem. J. 82 (2006) 43–48.
[40] C. Bouchelta, M.S. Medjram, O. Bertrand, J.P. Bellat, J. Anal. Appl. Pyrol. 82 (1) (2008) 70–77.
[41] A.B. Pérez Marín, M.I. Aguilar, V.F. Meseguer, J.F. Ortuño, J. Sáez, M. Lloréns, Chem. Eng. J. 155 (2009) 199–206.
[42] H. Arslanoglu, H.S. Altundogan, F. Tumen, Bioresour. Technol. 99 (7) (2008) 2699–2705.
[43] A. Sari, D. Mendil, M. Tuzen, M. Soylak, Chem. Eng. J. 144 (1) (2008) 1–9.
[44] M.A. Taher, S.E. Jarelnabbi, B.E. Bayoumy, S.M. El-Medani, R.M. Ramadan, Hindawi Publishing Corporation International Journal of Inorganic Chemistry, 2010, p. 6 (Article ID 296215) doi: http://dx.doi.org/10.1155/2010/296215.
[45] V. Murphy, S. Tofail, H. Hughes, P. McLoughlin, Chem. Eng. J. 148 (2009) 425–433.
[46] Medusa Program (Make Equilibrium Diagrams Using Sophisticated Algorithms, version 18 November 2008). Ignasi Puigdomenech, Inorganic Chemistry, Royal Institute of Technology (KTH), SE-100 44 Stockholm, Sweden. <http://www.kemi.kth.se/medusa> (accessed April 2011).
[47] M. Gorgievski, D. Bozíc, V. Stankovíc, N. Strbac, S. Serbula, Ecol. Eng. 58 (2013) 113–122.
[48] A. Hawari, Z. Rawajfih, N. Nsour, J. Hazard. Mater. 168 (2009) 1284–1289.
[49] S. Lagergren, Handlingar 24 (1898) 1–39.
[50] A. Bhattacharya, C. Venkobachar, J. Environ. Eng. 110 (1984) 110–122.
[51] W.J. Weber, J.C. Morris, J. Sanit. Eng. Div. ASCE 89 (1963) 31–59.
[52] Y.S. Ho, G. McKay, Process Biochem. 38 (2003) 1047–1061.
[53] Y. Sag, T. Kutsal, Process Biochem. 35 (2000) 801–807.
[54] J.M. Smith, Chemical Engineering Kinetics, third ed., McGraw-Hill, New York, 1981.
[55] I. Langmuir, J. Am. Chem. Soc. 40 (9) (1918) 1361–1403.
[56] T.W. Weber, R.K. Chakravorti, J. Am. Inst. Chem. Eng. 20 (1974) 228–238.
[57] H.M.F. Freundlich, Z. Phys. Chem. 57 (1906) 385–470.
[58] M.M. Dubinin, L.V. Radushkevich, Proc. Acad. Sci. U.S.S.R. Phys. Chem. Sect. 55 (1947) 331.
[59] S.S. Dubey, R.K. Gupta, Sep. Purif. Technol. 41 (2005) 21–28.
[60] A. Sarı, D. Cıtak, M. Tuzen, Chem. Eng. J. 162 (2010) 521–527.
[61] L. Al-Khateeb, A. Obaid, N. Asiri, M. Salam, J. Ind. Eng. Chem. 20 (2014) 916–924.
[62] A. Kilislioglu, B. Bilgin, Appl. Radiat. Isotopes 50 (2003) 155–160.
[63] S. Chen, Q. Yue, B. Gao, Q. Li, X. Xu, Chem. Eng. J. 168 (2011) 909–917.
[64] E. Malkoc, Y. Nuhoglu, Sep. Purif. Technol. 54 (2007) 291–298.
[65] S.K. Milonji, J. Serb. Chem. Soc. 72 (2007) 1363–1367.
[66] P. Suksabye, P. Thiravetyan, J. Environ. Manage. 102 (2012) 1–8.
[67] A. Albadarin, C. Mangwandi, G. Walker, S. Allen, M. Ahmad, M. Khraisheh, J. Environ. Manage. 114 (2013) 190–201.
[68] Y. Liu, Y.J. Liu, Sep. Purif. Technol. 61 (2008) 229–242.
[69] R.M. Schneider, C.F. Cavalin, M.A. Barros, C.R. Tavares, Chem. Eng. J. 132 (2007) 355–362.
[70] S. Sircar, R. Mohr, C. Ristic, M.B. Rao, J. Phys. Chem. B 103 (1999) 6539–6546.
[71] S. Sircar, Appl. Surf. Sci. 252 (2005) 647–653.
[72] M.R. Unnithan, T.S. Anirudhan, Ind. Eng. Chem. Res. 40 (2001) 2693–2701.
[73] I.X.G. García-Zubiri, G. González-Gaitano, J.R. Isasi, J. Colloid Interface Sci. 307 (2007) 64–70.
[74] D. Sud, G. Mahajan, M.P. Kaur, Bioresour. Technol. 99 (2008) 6017–6027.
[75] A.B. Albadarin, C. Mangwandi, A.H. Al-Muhtaseb, G.M. Walker, S.J. Allen, M.N.M. Ahmad, Chin. J. Chem. Eng. 20 (2012) 469–477.
[76] G.S. Bohart, E.Q. Adams, J. Chem. Soc. 42 (1920) 523–529.